Lab on a Chip

View Online
Dynamic Article Links

Cite this: *Lab Chip*, 2011, **11**, 1952

www.rsc.org/loc

PAPER

Ultrasensitive protein detection using lithographically defined Si multi-nanowire field effect transistors†

Ruhai Tian,[ab] Suresh Regonda,[a] Jinming Gao,[b] Yaling Liu[c] and Walter Hu*[a]

Received 16th November 2010, Accepted 18th March 2011
DOI: 10.1039/c0lc00605j

Low-doped silicon multi-nanowire field effect transistors with high ON/OFF ratio over 10^7 and a low subthreshold swing of 60–120 mV dec^{-1} are fabricated using lithographic semiconductor processes. The use of multi-nanowires instead of a single nanowire as sensing elements has shown improved device uniformity and stability in buffer solutions. The device stability is further improved with surface silanization and biasing with a solution gate rather than a backgate. pH sensing with a linear response over a range of 2–9 is achieved using these devices. Selective detection of bovine serum albumin at concentrations as low as 0.1 femtomolar is demonstrated.

Electrically biased bio-sensors using functionalized silicon nanowires,[1–3] carbon nanotubes,[4,5] and metal oxide nanowires/nanotubes[6–9] are emerging as powerful tools to quantify biochemical markers of low abundance with high sensitivity, which is critical to many disciplines in life sciences and health care, from disease diagnosis to drug discovery, as well as environment monitoring and bioterrorism. The advantages of nanowire biosensors include ultra-sensitivity, label-free and real-time detection, and small form factor.[10,11] The high sensitivity is attributed to small diameters of nanowires which are comparable to the device Debye length and size of biomolecules. For small nanowires, the entire channel can be fully modulated by binding of a small number of biomolecules.[12] Although sensing of low concentrations of proteins has been demonstrated with single nanowire field effect transistors (NW-FETs),[1,2] achieving device uniformity/reproducibility and stability in solution remains a challenge, making it difficult for applications involving complex biological samples *e.g.* whole blood, serum, and saliva. Device uniformity and reliability are important for the practical use of sensor arrays and for repeated sensing.

Device uniformity and reliability strongly depend on intrinsic device properties, fabrication techniques, and integrity of the bio–abio interface. One factor that may be overlooked in the field is the doping effect on intrinsic device properties. Studies[13,14] have shown that low level channel doping is important to achieve high sensitivity and has been widely used.[2,12] Unfortunately, because of a small volume of nanowire, low doping causes random variations in device performance due to the random arrangement of discrete dopants. This is known as discrete dopant fluctuation, *i.e.*, inconsistent distribution of dopants from wire-to-wire.[13,15–17] Device reproducibility is also related to fabrication techniques. For example, with chemically synthesized nanowires, it is difficult to have precise control of the nanowire size, doping uniformity, defects, and alignment on surfaces for device integration.[18] As a result, the device-to-device variations are large.[19] Recently, several groups have reported the use of CMOS compatible top-down lithography such as e-beam lithography (EBL) to make nanowires with well-controlled geometry and properties.[2,3,20,21] However, these devices using single nanowires with low doping are still subject to the aforementioned discrete doping effects and instability in solutions.[2,22,23]

Here, we report the use of EBL defined multiple Si nanowires (multi-SiNWs) in parallel configuration as sensing elements, together with improved interface and solution biasing to significantly improve the device stability and reliability while maintaining a high sensitivity. Previously, high-density SiNW arrays have been used for biosensing.[24,25] The reason of using NW arrays is due to their fabrication process of using superlattice nanowire pattern (SNAP) transfer[24] or grating mold in nanoimprint.[25] However, our rationale of explicitly using multi-NWs as a sensing element instead of a single NW is aimed to reduce discrete dopant fluctuation. We found that multi-SiNW FETs provide less performance variations and better stability in comparison with single nanowire FETs fabricated on the same chip using the same process, since multi-SiNWs accumulate and average the signal outputs of individual nanowires, making them less sensitive to discrete dopant fluctuations and interference from the environment. Moreover, multiple-wires offer higher drive current to

[a]*Department of Electrical Engineering, University of Texas at Dallas, Richardson, TX, 75080, USA. E-mail: walter.hu@utdallas.edu; Tel: +1 972 883 6329*
[b]*Department of Pharmacology, Simmons Comprehensive Cancer Center, University of Texas, Southwestern Medical Center, Dallas, TX, 75390, USA*
[c]*Department of Mechanical Engineering and Mechanics Bioengineering Program, Lehigh University, USA*

† Electronic supplementary information (ESI) available: Device surface modification details and control experiment of BSA sensing with bare devices. See DOI: 10.1039/c0lc00605j

improve the signal-to-noise ratio and reduce the complexity of readout circuits. We also found that using solution gate biasing to replace the traditional backgate configuration results in better stability and lower threshold voltage (V_t). Self-assembled monolayer (SAM) coatings can protect the gate oxide from ion penetration and interaction with buffer solution, leading to lower leakage current and much less device degradation. As a result of these improvements, we demonstrate stable multi-SiNW FETs in buffer solution. After specific surface functionalization, we show pH sensing with a linear response over a range of 2–9, and selective detection of bovine serum albumin (BSA) proteins at concentrations as low as ~0.1 femtomolar (fM).

The multi-SiNW FET devices are fabricated by e-beam lithography followed by reactive-ion-etching of an active silicon layer on silicon on insulator (SOI) substrates.[26] As shown in Fig. 1a, the devices are then packaged with on-chip microfluidic channels. p-Type SOI wafers with a 70 nm top Si layer (doped with boron at 10^{15} cm^{-3}) were cleaned with piranha (1 : 3 volume ratio of 30% H_2O_2 and 98% H_2SO_4), SC1 (1 : 1 : 5 volume ratio of 30% H_2O_2, 28% NH_4OH and H_2O) and SC2 (1 : 1 : 5 of 30% H_2O_2, 37% HCl and H_2O) solutions for 10 minutes, respectively. Then microscale Si pads were made with Cl_2 plasma etching (bias power of 150 W, rf power of 50 W at 5 mTorr pressure using an Oerlikon ICP etcher). The source and drain pads were then highly doped with phosphorus (10^{19} cm^{-3}) to form source/drain (S/D) junctions and facilitate low contact resistance. SiNWs were obtained by transferring e-beam defined hydrogen silsesquioxane (HSQ) lines using a two-step Cl_2 plasma etching.[26] 3–6 nm thick thermal oxide was formed on Si in a furnace at 900 °C. Metal contacts were fabricated by deposition of Ti/Al metal layers onto S/D pads. To avoid possible electrochemical reaction during sensing, the metal pads were fully passivated with ~170 nm thick Si_3N_4. Finally, the devices were annealed in forming gas (10% hydrogen in nitrogen) at ~450 °C for 30 minutes to make reliable metal/silicon ohmic contact and to minimize the interface states and fixed charges in the gate oxide. The sensing setup was

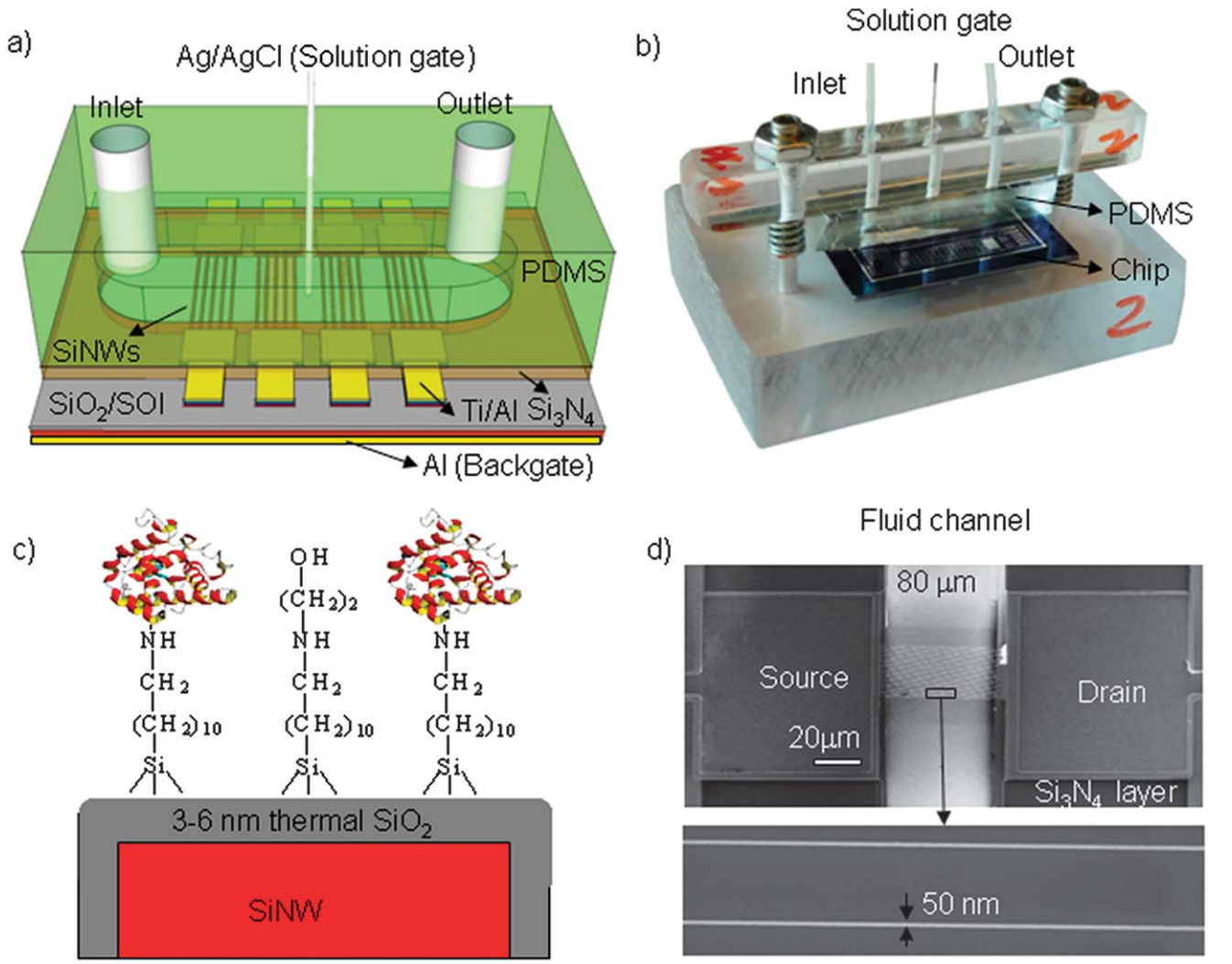

Fig. 1 (a) Schematic diagram of the multi-SiNW bio-FETs with an integrated PDMS fluidic channel, Ag/AgCl wire as a solution gate, and Si substrate as a backgate; (b) a picture of an assembled multi-SiNW FET sensing platform; (c) schematic of surface functionalization of SiNWs with TESU and anti-BSA (Not drawn in scale) and (d) SEM image of a multi-SiNW FET device containing 25 nanowires (50 nm in width) in parallel connected to source and drain (Ti/Al) pads.

designed and assembled as shown in Fig. 1a and b. Polydimethylsiloxane (PDMS) with a micro-machined fluidic channel and inlet/outlet ports was aligned and brought into contact with the SiNW chip and sealed using a mechanical clamp. The fluidic channel is 500 μm wide, 1.1 cm long, and 500 μm in height. The flowing rate was set at 5 ml h^{-1}, and there are about ~1000 target biomolecules flowing over the sensor per second at 1 fM analyte concentration. A metal wire (Ag/AgCl) was inserted through the PDMS into the solution serving as the solution gate. Fig. 1c shows the close-up view of the nanowire cross-section with surface functionalization for BSA sensing. All the nanowires were covered with 3–6 nm thermal SiO_2 serving as the dielectric layer. This oxide layer can prevent the direct contact of the buffer solution with Si which can degrade nanowire devices. This thermal oxidization process also reduces SiO_2/Si interface charges resulted from plasma etching (lower V_t and smaller subthreshold swing (SS) were observed after thermal oxidation). Nanowire surfaces were silanized with aldehyde terminated silanes.[27] These aldehyde groups were employed to anchor anti-BSA protein onto nanowire surfaces. Fig. 1d shows a scanning electron microscopic (SEM) image of twenty five nanowires in parallel, connected to Ti/Al pads. Using lithography, the geometry and placement of these nanowires can be precisely controlled. Because of using multiple instead of single nanowires in the FETs, the drive current is much higher, which allows us to use long nanowires (20–80 μm) and large sensing area to increase bimolecular binding from solution. The long nanowire also allows the use of a thicker passivation layer and microfluidic channel construction. Previous work of lithographic nanowires mostly uses short and single nanowires. Therefore we represent a different sensor design to achieve the similar sensitivity. The Si substrate underneath the nanowires was used as the backgate to measure the I_d–V_g curves. The low gate leaking current, ~10^{-11} A, high ON/OFF ratio of >10^7, subthreshold swings as low as 60–100 mV dec^{-1}, and electron mobility of >350 cm^2 V^{-1}·s are obtained.

As we have pointed out earlier, achieving device stability and high performance in buffer solutions is vitally important for using NW-FETs in biosensing. The high salt concentration in solution poses a challenge for the device stability since mobile ion contamination is known as a constant threat to semiconductor device performance and reliability. Time-dependent instability was widely observed in previous NW biosensors. Here we investigate the device performance in buffer solutions and their stability for different numbers of nanowires as well as various surface and bias conditions. Single nanowire FETs (same process on the same chip with multi-NW FETs) show instability and high noise in I_d–V_g curves when exposed to a solution for even a short time. Fig. 2a shows I_d–V_g curves of a single nanowire tested multiple times (length = 35 μm, width = 50 nm) in a buffer solution with solution gate. The I_d–V_g curve shifted uncontrollably and the device broke down in the second scan when I_g was larger than I_d. In fact, many single-NW devices broke down during the initial scan in the buffer solution. In comparison, Fig. 2b shows results of a multi-NW device (length = 50 μm, width = 50 nm, thickness = 30 nm) tested multiple times in different solutions. The device shows consistent stability in different concentrations of buffer solutions. The slight shifts of the I–V curves are due to the surface charge screening effects induced by different salt concentrations of the solutions. Moreover, from the perspective of device fabrication, we found the yield for single nanowire devices (<25% for 50 devices) is much lower than that of multi-NW devices (>75% for 100 devices) even when they were fabricated on the same chips with the same processes.

In addition to the number of nanowires, our experiments also show that both device performance and stability strongly depend on the gate biasing, *e.g.*, biasing at the Si substrate underneath nanowires (backgate) *vs.* biasing through an electrode in the solution (solution gate). Fig. 3a shows the comparison of device I_d–V_g curves in the buffer solution under backgate and solution gate biasing. For both biasing conditions, the device shows a similar ON/OFF ratio of ~10^8 and a similar subthreshold swing (109 and 121 mV dec^{-1} for back and solution gates, repetitively). These results indicate good integrity of the dielectric (stable Si/SiO_2 interface) and successful passivation of metal pads. The biasing configuration (backgate or solution gate) does not have strong effects on the device subthreshold swing (SS), which is expected. SS is expressed as the following equation: $SS = (\ln 10)(kT/q)[(C_{ox} + C_D)/C_{ox}] = 59.3(1 + C_D/C_{ox})$, where kT is the thermal energy at room temperature; C_{ox} is the gate-oxide capacitance and C_D is the depletion layer capacitance. For our NW-FET geometry, C_D is significantly smaller than the C_{ox} for both backgate and solution gate configurations, and therefore the device SS is not affected by the biasing configurations. The first major difference between solution gate and backgate we have observed is the V_t, 1.7 V for solution gate and 3.7 V for backgate. Smaller V_t for solution gate is due to the thinner gate oxide (6 nm) compared to the buried oxide (BOx) of 145 nm. Low V_t allows low biasing voltage which is helpful to maintain the stability during sensing since high gate voltage can potentially degrade the Si/SiO_2 interface.[28] The second difference is that when the backgate bias was applied, we never got time-dependent stable current under constant gate biasing. As shown in Fig. 3b, the drain current drops dramatically (within 5 minutes), inhibiting the use for biosensing. However, when the solution gate was employed to bias the devices, the drain current was stable for at least 2 hours, which is critical for reliable biosensing. Others also reported baseline current instability for backgate biasing.[22] We believe this time-dependent instability may likely be attributed to the large capacitive coupling between solution in the microfluidic channel and the backgate, and possibly the pinhole defects in the BOx layer.

We have also found that the SAMs anchored on the SiO_2 serve as not only a linker for antibody immobilization but also a protective layer to prevent the direct contact of the buffer solution with oxide surfaces. We found this silanization process of the device surfaces using SAMs reduces device degradation. Fig. 4a shows the device performance without SAM coating before and after solution gate bias at 0.7 V for 30 minutes in the buffer solution (0.1 mM phosphate buffer solution or PBS/0.1 mM NaCl). The gate current increases dramatically about three orders. In comparison, after the device surfaces are silanized with 11-(triethoxysilyl)undecanal (TESU) molecules, the gate current remains nearly the same even after biasing at 0.7 V for 130 minutes (Fig. 4b). The improved device stability is attributed to the protection of gate oxide surfaces by the hydrophobic silane from salty water contact and erosion, as proven by our FTIR analysis (ESI†, Fig. S1).

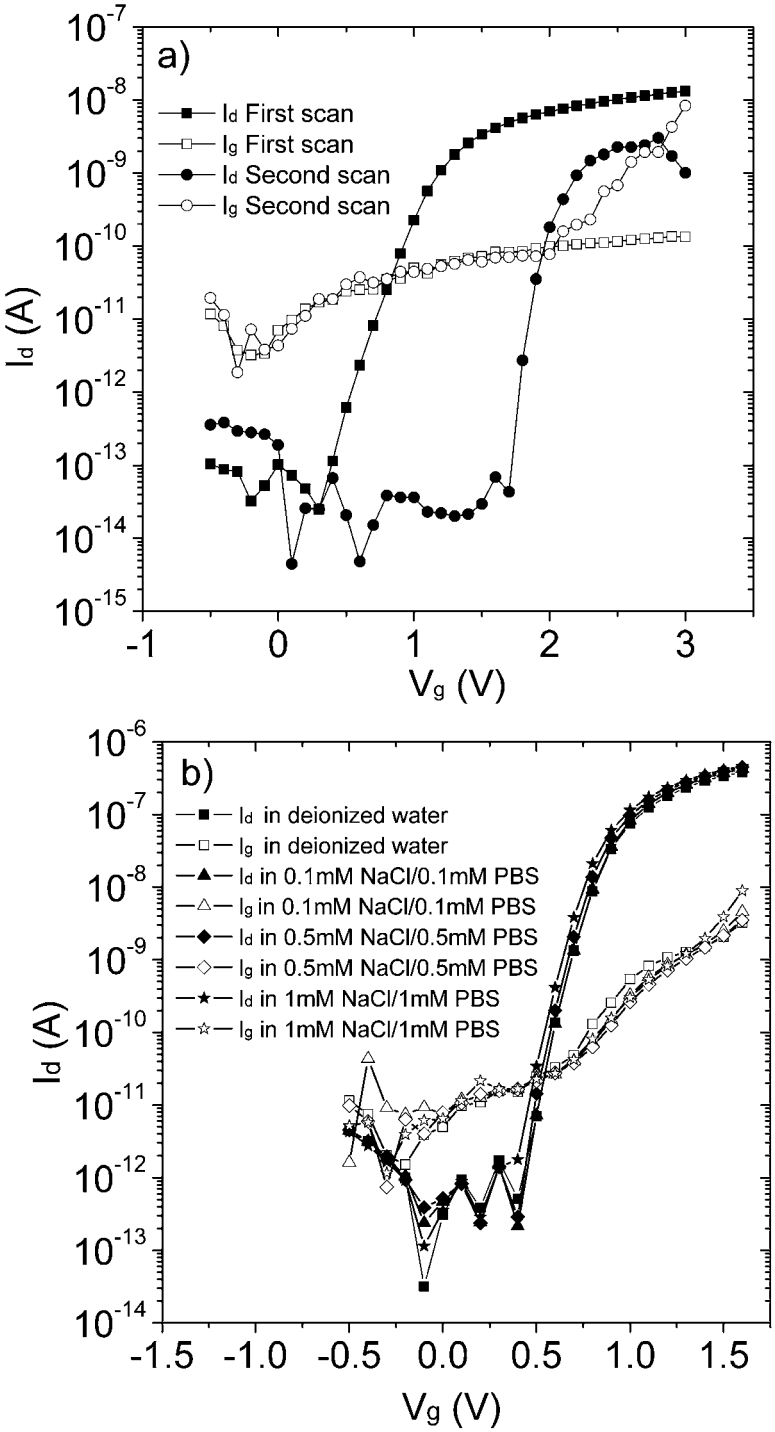

Fig. 2 (a) I_d–V_g curves for single nanowire device (length = 35 μm, width = 50 nm) with multi-scans in the buffer solution (1 mM NaCl/1 mM PBS, pH 7.4) and (b) I_d–V_g curves for multi-SiNW FETs (length = 50 μm, width = 50 nm, number = 50) in different concentration of buffer solutions. The device shows stable high performance.

To demonstrate sensing with the multi-SiNW FETs, we first studied the pH sensing in a range of 2–9. As shown in Fig. 1a, a flow-through microfluidic system was used for sample delivery. We used buffer solutions with high salt concentration (10 mM PBS, 0.1 M NaCl) to eliminate the possible effects of the variation of ion concentration for different pH values.[29] Since a lot of previous work used SiO_2 directly as a sensing element in ion sensitive FETs (ISFETs), here we investigate pH sensing using devices with and without SAM coating. The devices were biased at the strong inversion region for high current during pH sensing to cover a wide pH range. Even though the gate leakage current is high for devices without SAMs, the drain current is considerably higher than the leakage current, allowing us to perform pH sensing using the device without SAMs as a comparison. Fig. 5a

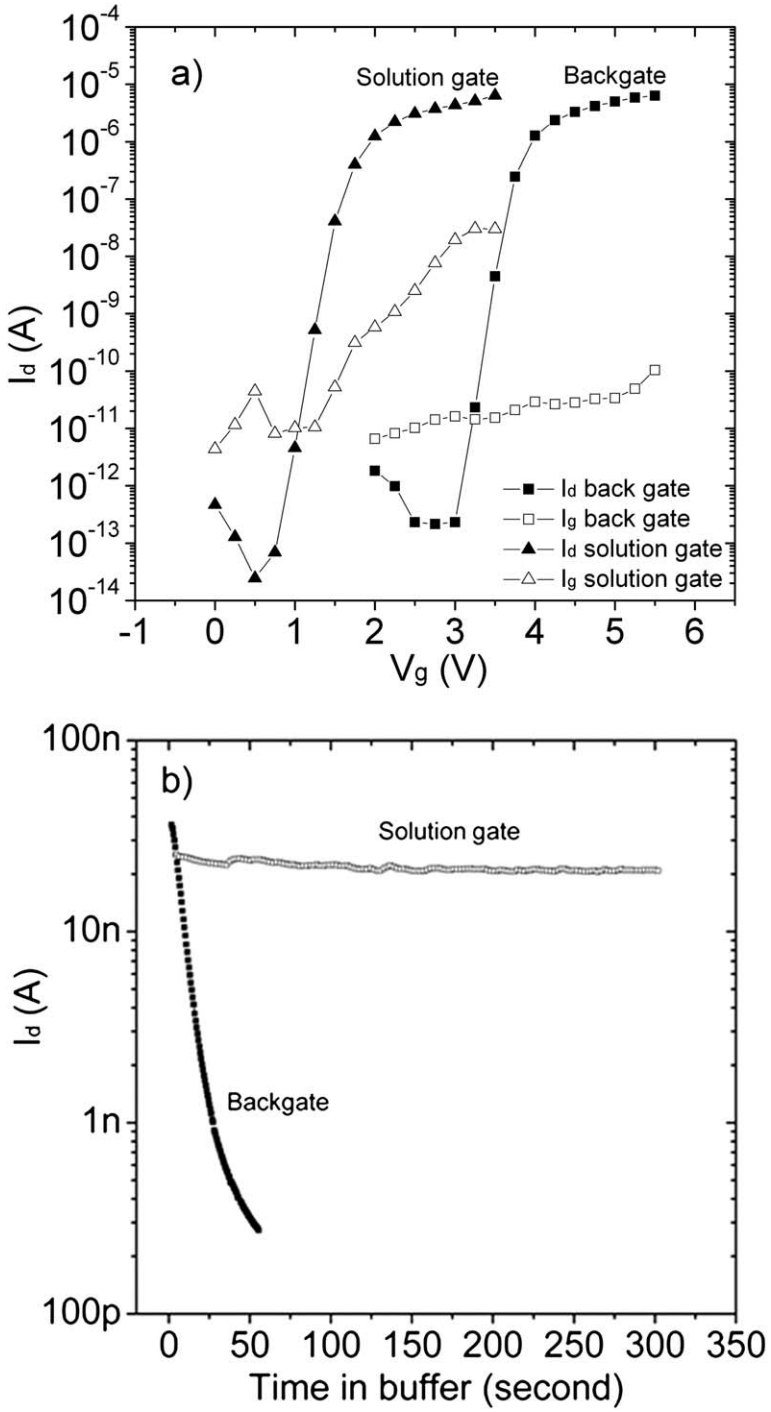

Fig. 3 Comparison of device performance and stability in the buffer solution (10 mM PBS, pH 7.4) with backgate *vs.* solution gate biasing: (a) I_d–V_g curves of the same device containing 50 nanowires with a width of 160 nm and a length of 80 μm under backgate and solution gate biasing and (b) time-dependent current stability (I_d–time curve) with backgate *vs.* solution gate biasing for the same device.

shows the device conductance during sequential injection of solutions with varying pH values (2–9 with discrete step of 1) for multi-SiNW FETs without SAMs. The result shows that the device is only sensitive to the solution pH in a range of 5–11. In addition, the drain current steps are not stable for fixed pH values, which may be due to the aforementioned unstable performance of devices without SAM protection.

For another multi-SiNW FET, the SiO_2 surface was modified with 3-aminopropyltriethoxysilane (APTES). Previous work has shown APTES coated ISFET provides linear response to pH which is different from bare SiO_2.[1] We also observe linear response of the drain current with pH values ranging from 2.0 to 9.0, which is shown in Fig. 5b. The drain current for the same pH solution is stable due to protection of gate oxide by the APTES.

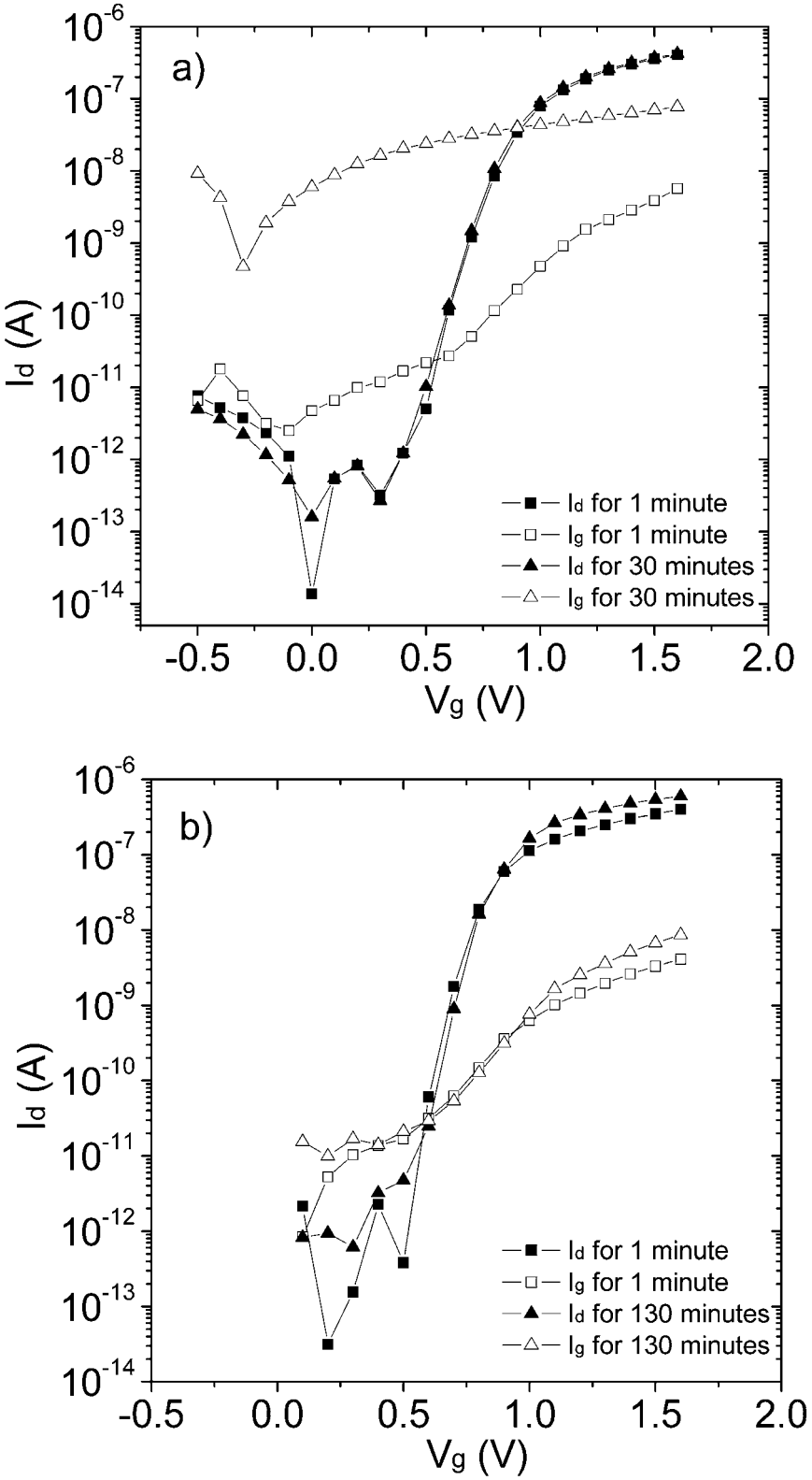

Fig. 4 I_d–V_g curves and gate leakage current (I_g) of multi-SiNW FETs in the buffer solution (0.1 mM PBS/0.1 mM NaCl, pH 7.4): (a) device without SAM surface coating on NWs with one min *vs.* 30 min in solution under fixed solution gate biasing at 0.7 V for sensing; the device contains 50 nanowires with a length of 50 μm and a width of 23 nm and (b) device with TESU surface coating on NWs with one min *vs.* 130 min in solution under fixed solution gate biasing at 0.7 V. The device contains 25 nanowires with a length of 50 μm and a width of 45 nm.

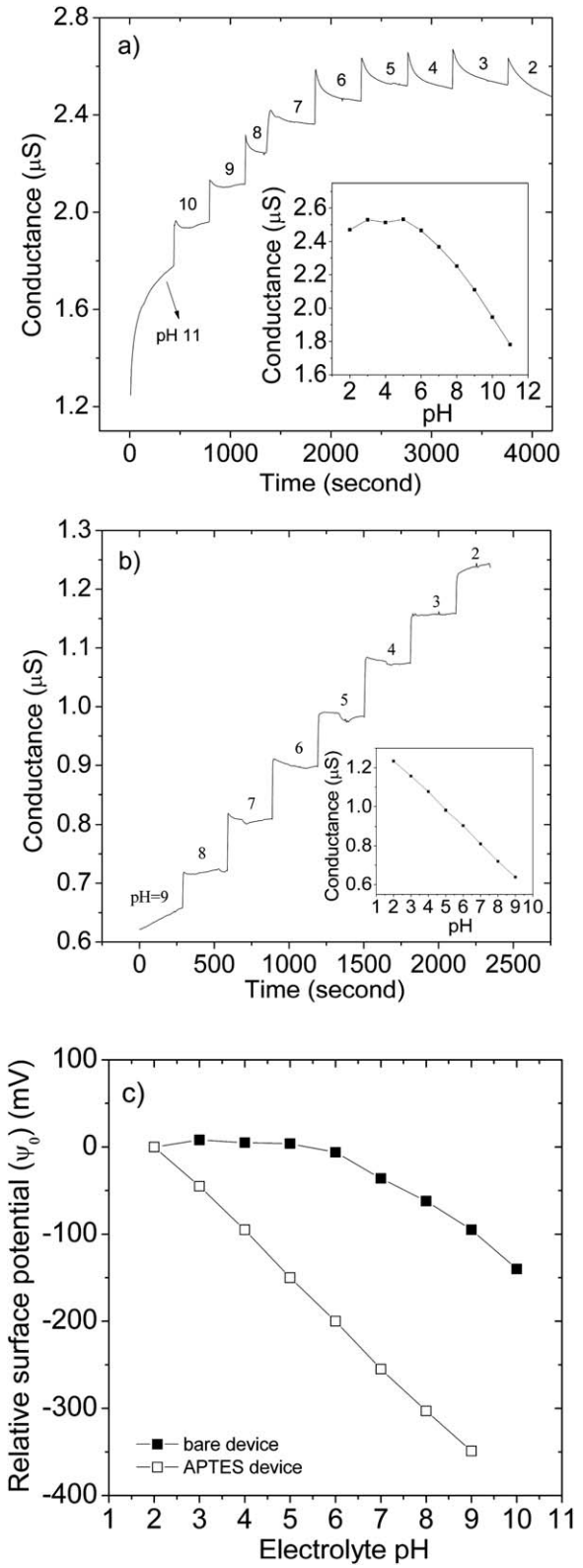

Fig. 5 pH sensing results using multi-SiNW FETs biased with solution gate in the strong inversion region: (a) NWs without SAM coating (NW length = 80 μm, width = 130 nm, wire number = 25) and (b) NWs with APTES surface coating (NW length = 80 μm, width = 60 nm, wire number = 25). The insets show the device conductance as a function of pH. (c) The relative device surface potentials due to pH changes, extracted from I_d–pH curves and I_d–V_g curves, for devices with and without APTES coating.

The mechanism of NW-FETs (or ISFET in general) response to ions has been intensively discussed in literatures.[30–32] The linear relation between the nanowire surface potential (ψ_0) and solution pH is responsible for the linear pH response since the drain current is directly proportional to the surface potential.[31,33] The pH sensitivity of ISFET can be expressed as:

$$\frac{\delta\psi_0}{\delta \mathrm{pH}_B} = -2.3\frac{kT}{q}\alpha \quad (1)$$

$$\alpha = \frac{1}{\left(2.3kTC_{\mathrm{dif}}\Big/q^2\beta_{\mathrm{int}}\right)+1} \quad (2)$$

where k is the Boltzmann constant; T is the absolute temperature; C_{dif} is the differential double-layer capacitance; and β_{int} is the intrinsic surface buffer capacity of the dielectric material surface (SiO_2 for bare device).[31] The pH sensing indicates the I_d is linear to ΔpH when the SiO_2 surface is modified with amino groups. From the I_d–V_g and I_d–pH curves, the relative surface potential changes $\Delta\psi$ (reference to data point at pH 2.0) were extracted, as shown in Fig. 5c. It clearly shows a linear correlation between the surface potential and ΔpH (~50 mV per pH), indicating APTES coated surface has a constant α value (~0.85) in eqn 2. In contrast, the surface potential *vs.* solution pH relationship for devices without SAMs is not linear, indicating that α is a variable factor, *e.g.* ~0.07 at low pH and ~0.93 for high pH. This study is consistent with previous experimental and theoretical studies on bare SiO_2[34] and APTES modified SiO_2 materials.[35] Most importantly for us, the pH sensing results prove that the multi-SiNW FETs with SAM coating are reliable platforms for sensing the surface charge, which is a key checkpoint before we perform protein detection.

Our motivation for developing stable SiNW bioFETs is to detect proteins in solution. As discussed earlier, protein detection at ultralow concentrations such as fM in solution is critical for early diagnostics of many diseases. In biosensing, the limit of detection (LOD), defined as the lowest detectable molar concentration of proteins, is used as a primary measure of sensitivity.[36,37] Previously, LOD at the fM level has been demonstrated by single-SiNW devices.[38,39] Here we investigate the sensitivity and LOD of multi-SiNW-FET devices under measurable signal-to-noise ratios. Although we aim to detect disease-signature biomarkers eventually, BSA protein was used in this study as a target with carbonate anhydrase (CA) as the interferent since they are widely used in the literature and both proteins have a similar charge.

Different from pH sensing, where proton concentration is high (1×10^{-10} M and 1×10^{-2} M for pH 10 and 2, respectively), protein detection at low concentrations (~fM) requires higher device sensitivity. Therefore we biased our device at the subthreshold ($V_g < V_t$) region to maximize the device sensitivity.[12] The nanowire surfaces were first treated with piranha solution for 15 seconds to obtain clean and hydrophilic surfaces. Then the device surfaces were silanized by immersion of the device in a TESU solution (1% in anhydrous toluene) for 10 hours, followed by rinsing with toluene. Anti-BSA was immobilized onto the nanowire surfaces by the dipping of TESU functionalized devices in 50 μg ml^{-1} anti-BSA buffer solution (10

mM PBS, 10 mM NaCl, 5 mM $NaBH_3CN$) for about 5 hours. The un-reacted aldehyde groups were passivated with ethanolamine under similar conditions. These functionalized surfaces have been demonstrated by FTIR, AFM and contact angle measurements (ESI†, Fig. S1). Here we are using TESU instead of 3-(trimethoxysilyl)propyl aldehyde (TMSPA, a popular SAM in most previous work) as a protein linker because we found that TESU/SiO_2 is more stable than the TMSPA/SiO_2 surface. To ensure the target molecules can be detected, we used a low salt concentration buffer solution, 10 μM NaCl/10 μM PBS, which allows a Debye length >30 nm to avoid shielding effects.[22] To prove detection of BSA at the fM level, control experiments have been performed carefully. First, we have demonstrated the device without surface functionalization (SAMs and antibodies) is inert to the BSA proteins (ESI†, Fig. S2). Then the sensing of BSA was carried out with the anti-BSA anchored multi-SiNW FETs.

Fig. 6a shows the conductance changes of the NW devices when various solutions were injected. All curves have a similar baseline conductance of ~800 nS and they are discretely shown in the figure with the same scale for better visibility and comparison. First, we show the delivery of multiple pure buffer solutions without proteins does not cause conductance change. When various concentrations of BSA, 0.13 fM, 0.25 fM, and 0.5 fM BSA solutions, were delivered to the sensor, we observed decreases of nanowire conductance. The magnitude of the conductance change increases monotonically with the protein concentration. Since the BSA solution has a pH value of 7.4 which is higher than the isoelectric point (PI) of BSA (~5.0), the negative charges of BSA cause more depletion of electron carriers in the nanowires and decrease of device conductance for n-channel NW-FETs. The drain current recovers to the baseline as expected when the device is flushed with a buffer solution that removes the binding of BSA. It shows that the binding is reversible and the detection is repeatable. In order to demonstrate the BSA sensing is selective, 100 fM CA was delivered to the device surface and no drain current decrease was detected, which indicate CA protein does not bind to anti-BSA enough to cause a measurable signal. We also delivered a mixture solution of 0.5 fM BSA and 100 fM CA onto the device, which shows a slightly larger signal compared with pure 0.5 fM BSA sensing. For the lowest LOD, our experiment shows that 0.13 fM BSA solution can generate a measurable conductance decrease with a signal-noise ratio of ~3. Moreover, we performed similar tests for largely varied protein concentrations to study the dynamic range of detection. As shown in Fig. 6b, the sensitivity ($\Delta G/G$) is monotonically proportional to the BSA concentration for values from 0.1 fM to 1 pM. The control experiments using CA show that for the same $\Delta G/G$, *e.g.* 2%, the specificity of BSA concentration over CA concentration is ~5 orders of magnitude larger. The systematic tests of protein detection in buffer solutions show that with improved stability, multi-SiNW FETs are capable of selective detection of protein with LODs of sub-fM. We believe this attributes to the small SS of the devices and also the use of parallel multiple low-doped Si nanowires as stable sensing elements to allow attachment of a small number of proteins to modulate the entire conducting channel.

The detection time of our sensors is in seconds (~10 seconds), which is similar to other reported studies.[2,20,38,39] This short response time does not comply to the classic binding-affinity

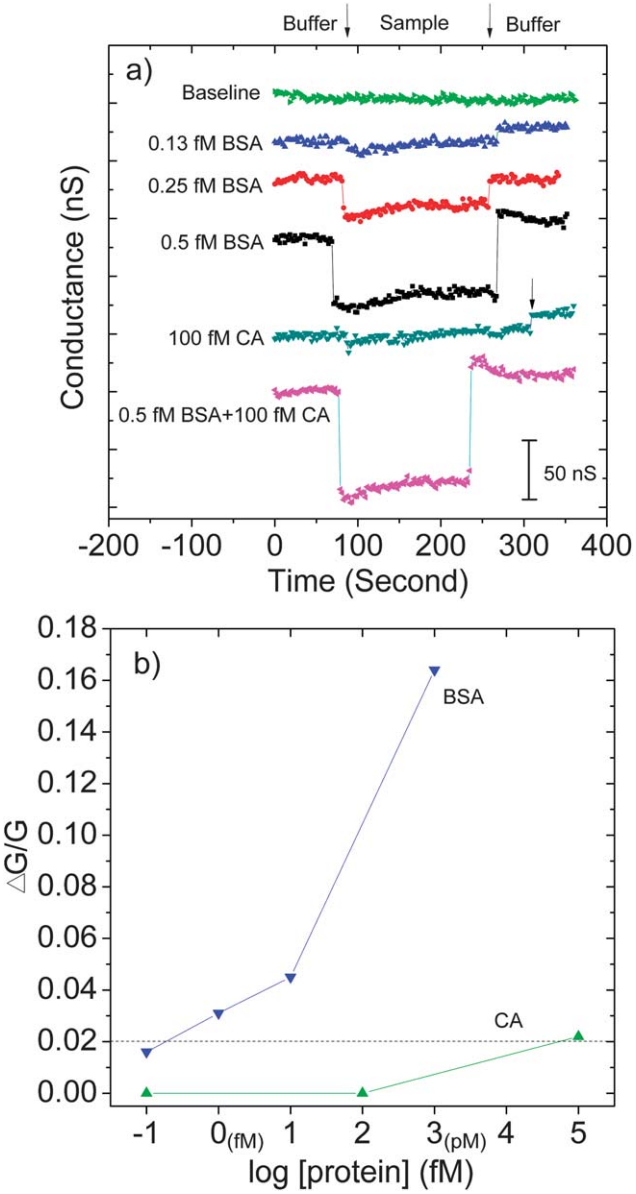

Fig. 6 Protein sensing results using multi-SiNW FETs: (a) NW conductance changes due to various concentrations of BSA proteins in solution with the same pH = 7.4 and salt concentration (10 mm PBS, 10 mM NaCl). All curves have the same baseline conductance of 800 nS. The device contains 25 nanowires with a length of 50 μm and a width of 45 nm. Multi-SiNW FETs show ultrahigh sensitivity to detect sub-fM BSA proteins. (b) The intrinsic sensitivity of multi-SiNW FETs as a function of molar concentrations of BSA *vs.* CA proteins, demonstrating over 5 orders of dynamic range and $>10^5$ selectivity for BSA detection over CA.

based model (thermodynamic diffusion of protein to sensing elements), which suggests much longer times (~hours) to reach the equilibrium protein concentration at the sensor surface at the fM level. This discrepancy on detection time (3 orders of magnitude difference) for nanowire biosensors has been widely reported between experimental observation (seconds to minutes) and simulation results (~hours).[40] We believe one major reason is the strong effect of applied electric fields on the dynamic transport of biomolecules, which can reduce the detection time by orders of magnitudes.[40] Here we show a preliminary study of

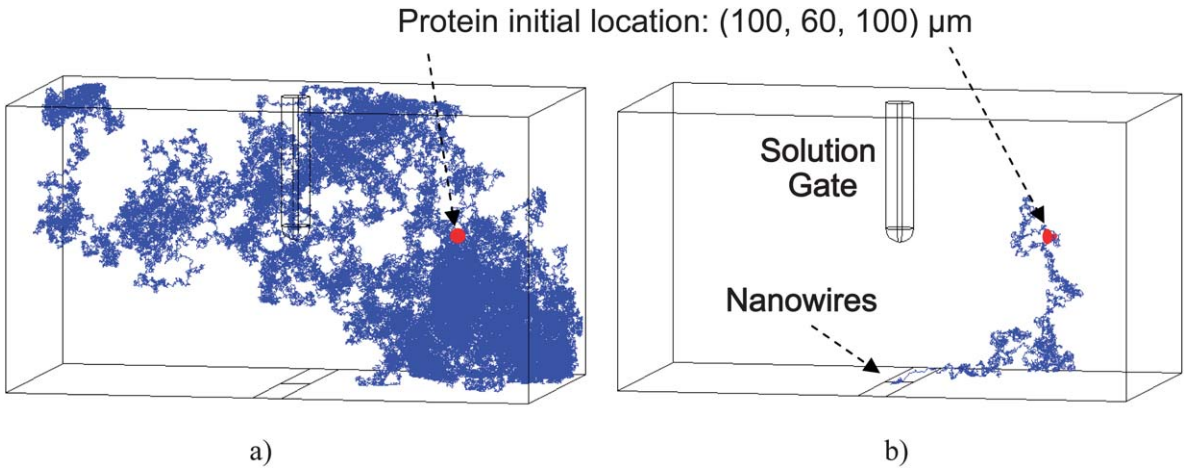

Fig. 7 Simulated trajectories of a biomolecule under: (a) pure Brownian motion and (b) Brownian motion and electrokinetics for our NW sensor geometry/architecture.

biomolecule transportation to the nanowire device surface under applied electric field using numerical simulation with the Brownian adhesion dynamic model together with consideration of electrokinetics. Fig. 7shows the simulated random trajectories of a charged biomolecule (*e.g.* protein) under pure Brownian motion (BM), and BM with electrokinetic effect (electrostatics and electroosmosis flow) for the exact geometry and architecture of our sensor. The initial position of the biomolecule in both cases is (100,60,100) in a domain of size 370 × 200 × 200 μm, similar to the protein density around fM concentration. In Fig. 7a, due to the randomness of the Brownian motion, biomolecules would travel around the whole domain before they get bonded with the nanowire sensor, thus the detection process takes a long time (at least a few hours). However, electrokinetic effects such as electrophoresis and electroosmosis can help biomolecules to concentrate near the sensor region and significantly improve the possibility of protein reaching the nanowire surface, which decrease the detection time dramatically to tens of seconds, as shown in Fig. 7b. A detailed model of the biosensing process at ultralow concentration with electrokinetic effect considered is described elsewhere.[41]

In summary, we have demonstrated fabrication of high-performance low-doped Si multi-NW FETs with long channel using a lithographic MOSFET process. These transistors show good uniformity, high ON/OFF ratio and small subthreshold swing. The use of multi-nanowires rather than single nanowire as sensing elements enables high device uniformity and stability in buffer solutions. The device stability is further improved with surface silanization and solution biasing rather than conventional backgate biasing. The devices have shown reliable pH sensing with excellent linearity and selective detection of BSA protein with a detection limit about 0.1 fM concentration. We believe the combination of high stability and high sensitivity by the multi-nanowire FETs is highly promising for label-free, real-time, and low cost biosensing applications.

Acknowledgements

The authors thank Krutarth Trivedi and Xinrong Yang for useful discussions. The research is supported by Texas Instrument Inc., Richardson, Texas, National Science Foundation (Career Award, ECCS-0955027), and National Institutes of Health.

References

1 Y. Cui, Q. Q. Wei, H. K. Park and C. M. Lieber, *Science*, 2001, **293**, 1289–1292.
2 E. Stern, J. F. Klemic, D. A. Routenberg, P. N. Wyrembak, D. B. Turner-Evans, A. D. Hamilton, D. A. LaVan, T. M. Fahmy and M. A. Reed, *Nature*, 2007, **445**, 519–522.
3 O. H. Elibol, D. Morisette, D. Akin, J. P. Denton and R. Bashir, *Appl. Phys. Lett.*, 2003, **83**, 4613–4615.
4 K. Besteman, J.-O. Lee, F. G. M. Wiertz, H. A. Heering and C. Dekker, *Nano Lett.*, 2003, **3**, 727–730.
5 J. Kong, N. R. Franklin, C. Zhou, M. G. Chapline, S. Peng, K. Cho and H. Dai, *Science*, 2000, **287**, 622–625.
6 Q. Wan, Q. H. Li, Y. J. Chen and T. H. Wang, *Appl. Phys. Lett.*, 2004, **84**, 3654–3656.
7 Z. Fan, D. Wang, P. Chang, W. Tseng and J. G. Lu, *Appl. Phys. Lett.*, 2004, **85**, 5923–5925.
8 M. Law, H. Kind, B. Messer, F. Kim and P. Yang, *Angew. Chem., Int. Ed.*, 2002, **41**, 2405–2408.
9 E. Comini, G. Faglia, G. Sberveglieri, Z. W. Pan and Z. L. Wang, *Appl. Phys. Lett.*, 2002, **81**, 1869–1871.
10 F. Patolsky, G. Zheng and C. M. Lieber, *Anal. Chem.*, 2006, **78**, 4260–4269.
11 E. Stern, A. Vacic and M. A. Reed, *IEEE Trans. Electron Devices*, 2008, **55**, 3119–3130.
12 X. P. A. Gao, G. Zheng and C. M. Lieber, *Nano Lett.*, 2010, **10**, 547–552.
13 P. R. Nair and M. A. Alam, *IEEE Trans. Electron Devices*, 2007, **54**, 3400–3408.
14 M. N. Masood, S. Chen, E. T. Carlen and A. v. d. Berg, *ACS Appl. Mater. Interfaces*, 2010, **2**, 3422–3428.
15 T. Mizuno, J.-i. Okamura and A. Toriumi, *IEEE Trans. Electron Devices*, 1994, **41**, 2216–2221.
16 A. Asenov, A. R. Brown, J. H. Davies, S. Kaya and G. Slavcheva, *IEEE Trans. Electron Devices*, 2003, **50**, 1837–1852.
17 D. Vasileska, W. J. Gross and D. K. Ferry, in *Proceedings of the 1998 Sixth International Workshop on Computational Electronics*, 1998, pp. 259–262.
18 B. K. Teo and X. H. Sun, *Chem. Rev.*, 2007, **107**, 1454–1532.
19 F. Patolsky and C. M. Lieber, *Mater. Today*, 2005, **8**, 20–28.
20 Y. Chen, X. H. Wang, S. Erramilli, P. Mohanty and A. Kalinowski, *Appl. Phys. Lett.*, 2006, **89**, 223512.
21 Z. Li, Y. Chen, X. Li, T. I. Kamins, K. Nauka and R. S. Williams, *Nano Lett.*, 2004, **4**, 245–247.

22 E. Stern, R. Wagner, F. J. Sigworth, R. Breaker, T. M. Fahmy and M. A. Reed, *Nano Lett.*, 2007, **7**, 3405–3409.
23 K. Trivedi, H. Yuk, H. C. Floresca, M. J. Kim and W. Hu, *Nano Lett.*, 2011, DOI: 10.1021/nl103278a.
24 Y. L. Bunimovich, Y. S. Shin, W.-S. Yeo, M. Amori, G. Kwong and J. R. Heath, *J. Am. Chem. Soc.*, 2006, **128**, 16323–16331.
25 A. A. Talin, L. H. Luke, L. Francois and R. Bhavin, *Appl. Phys. Lett.*, 2006, **89**, 153102.
26 S. Regonda, M. Aryal and W. Hu, *J. Vac. Sci. Technol., B*, 2008, **26**, 2247–2251.
27 R. Tian, O. Seitz, M. Li, W. W. Hu, Y. J. Chabal and J. Gao, *Langmuir*, 2010, **26**, 4563–4566.
28 E. K. Propst and P. A. Kohl, *J. Electrochem. Soc.*, 1994, **141**, 1006–1013.
29 D. R. Kim, C. H. Lee and X. Zheng, *Nano Lett.*, 2009, **9**, 1984–1988.
30 W. M. Siu and R. S. C. Cobbold, *IEEE Trans. Electron Devices*, 1979, **26**, 1805–1815.
31 Ir. P. Bergveld Em, *ISFET, Theory and Practice*, *IEEE Sensor Conference*, Toronto, 2003.
32 P. R. Nair and M. A. Alam, *Nano Lett.*, 2008, **8**, 1281–1285.
33 C. D. Fung, W. H. Ko and P. W. Cheung, *IEEE Trans. Electron Devices*, 1986, **ED-33**, 8–18.
34 P. M. Dove and C. M. Craven, *Geochim. Cosmochim. Acta*, 2005, **69**, 4963–4970.
35 A. A. Golub, A. I. Zubenko and B. V. Zhmud, *J. Colloid Interface Sci.*, 1996, **179**, 482–487.
36 D. MacDougall and W. B. Crummett, *Anal. Chem.*, 1980, **52**, 2242–2249.
37 G. L. Long and J. D. Winefordner, *Anal. Chem.*, 1983, **55**, 712A–724A.
38 G. Zheng, F. Patolsky, Y. Cui, W. U. Wang and C. M. Lieber, *Nat. Biotechnol.*, 2005, **23**, 1294–1301.
39 A. Kim, C. S. Ah, H. Y. Yu, J. H. Yang, I. B. Baek, C. G. Ahn, C. W. Park, M. S. Jun and S. Lee, *Appl. Phys. Lett.*, 2007, **91**, 103901.
40 T. M. Squires, R. J. Messinger and S. R. Manalis, *Nat. Biotechnol.*, 2008, **26**, 417–426.
41 Q. Guo, J. Tan, W. Hu and Y. Liu, 2011, in preparation.